Supplemental material

Wang et al., https://doi.org/10.1083/jcb.201712130

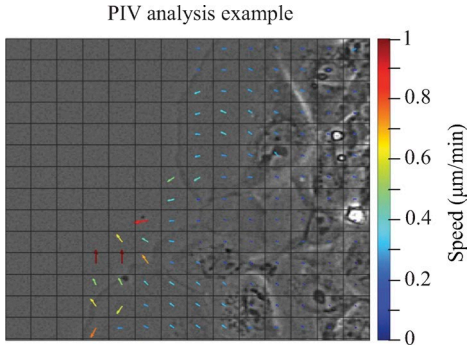

Figure S1. **PIV analysis was used to monitor the connective migration of keratinocyte sheet.** The example presented here is an analysis of WT keratinocytes migrating on laminin. Each arrow points toward the direction of movement and is color coded according to the scale displaying the speed of movement (μm/min).

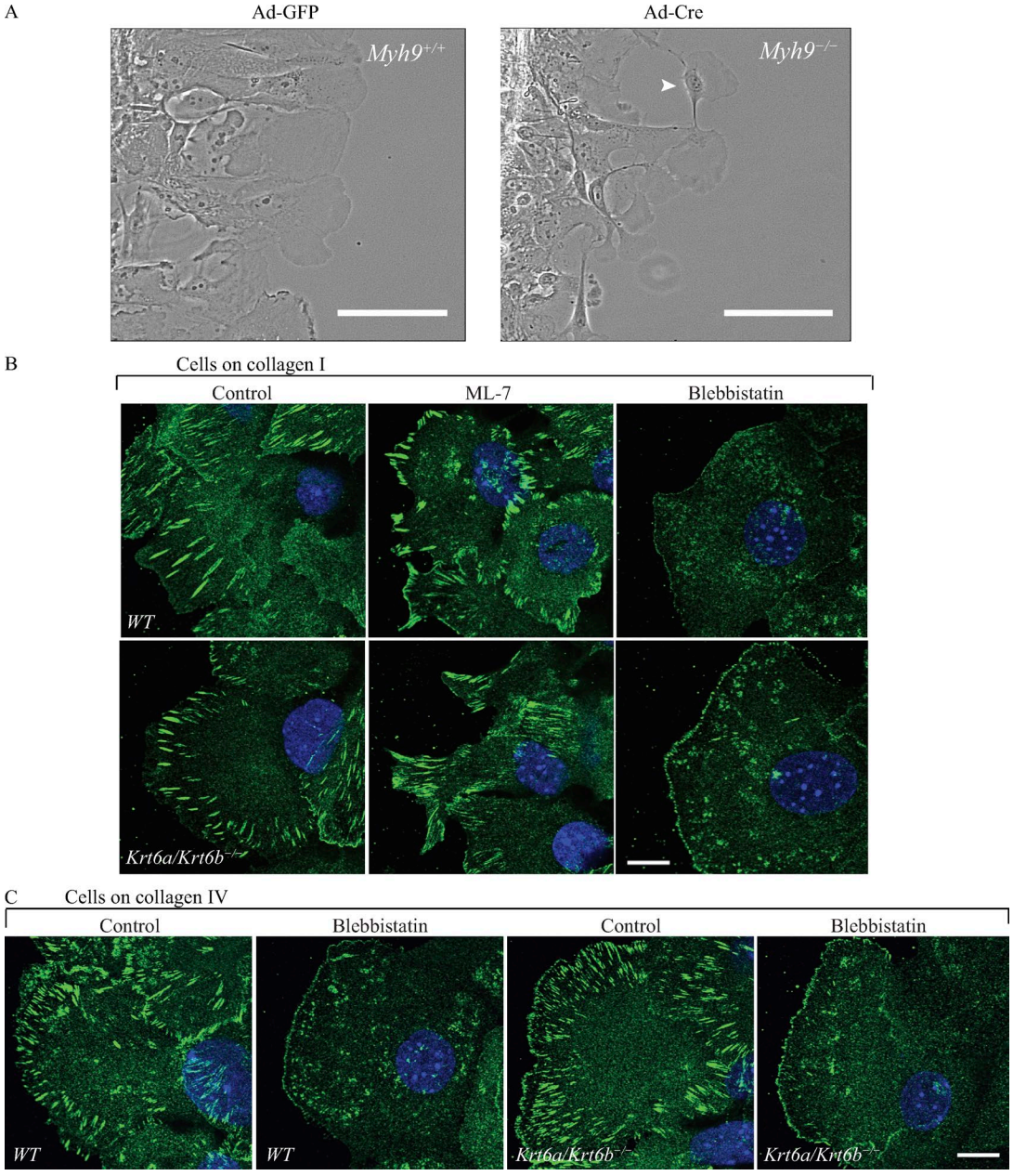

Figure S2. **Impact of disrupting myosin II function on cell–cell adhesion and focal adhesions. (A)** Genetically silencing *Myh9* disrupted cell–cell adhesion in cells at the migration front edge. The arrowhead points to a leader cell that is partially detached from follower cells (Video 6). **(B)** On type I collagen, treatment with the MLCK inhibitor ML-7 resulted in increased size of focal adhesions, whereas treatment with the myosin II inhibitor blebbistatin disrupted focal adhesion structures for both genotypes. **(C)** We noted that, when plated on type IV collagen, both WT and *Krt6a/Krt6b*-null keratinocytes had more focal adhesions than on type I collagen (B). Blebbistatin treatment disrupted focal adhesion structures for both WT and *Krt6a/Krt6b*-null migrating keratinocytes. All cells shown in these images were at the migration leading edge. Paxillin, green. DAPI, blue. Bars: 100 µm (A); 10 µm (B and C).

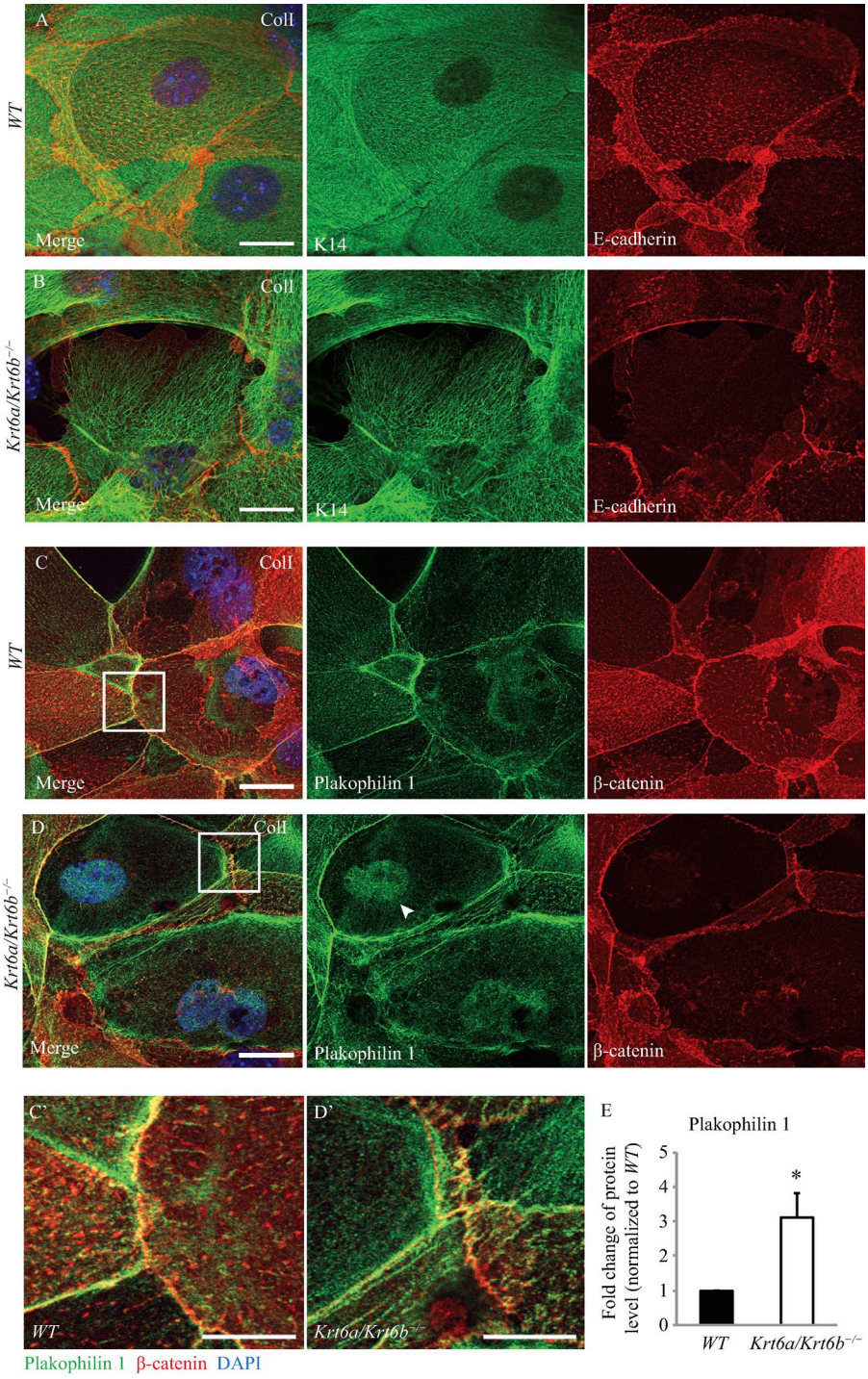

Figure S3. **The localization of E-cadherin, plakophilin 1, and β-catenin is disrupted with the loss of K6a/K6b in migrating *Krt6a/Krt6b*-null keratinocytes. (A and B)** The distribution of E-cadherin is altered in *Krt6a/Krt6b*-null keratinocytes on type I collagen. K14, green; E-cadherin, red; DAPI, blue. **(C and D)** Plakophilin 1 and β-catenin show reduced colocalization at cell–cell adhesion (C′ and D′) with the loss of K6a/K6b. A greater fraction of the plakophilin 1 signal localizes to the nucleus and cytoplasm in *Krt6a/Krt6b*-null keratinocytes on type I collagen. Arrowheads point to nuclear-localized plakophilin 1. Plakophilin 1, green; β-catenin, red; DAPI, blue. Bars: 20 µm (A–D) and 10 µm (C′ and D′). All cells shown in these images were adjacent to the migration leading edge. **(E)** Plakophilin 1 protein levels are increased in the absence of K6a/K6b. Quantification of Western blot results of six biological replicates. Data represent the mean + SEM. *, $P < 0.05$, Student's two-tailed *t* test.

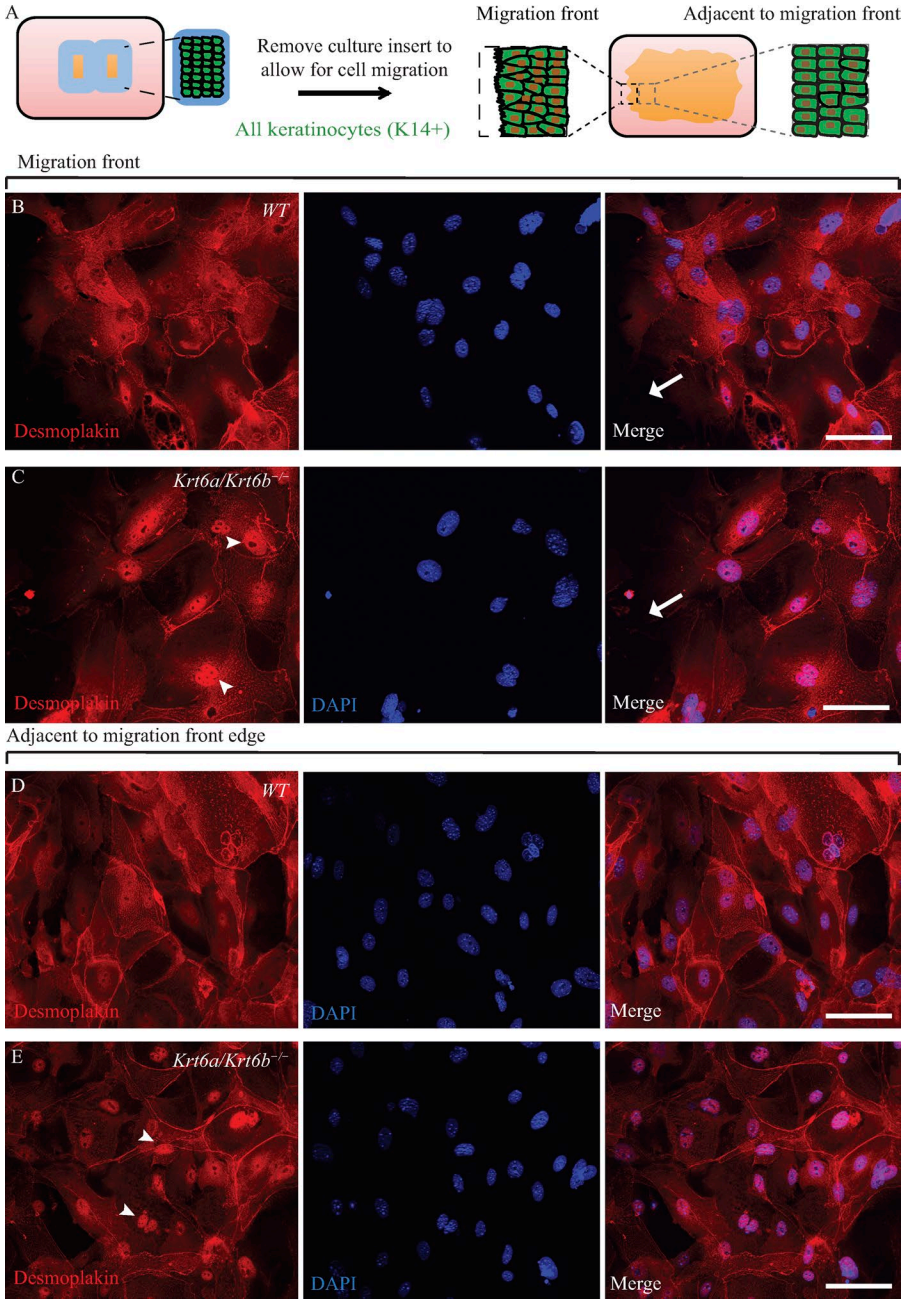

Figure S4. ***Krt6a/Krt6b*-null keratinocytes showed prominent intranuclear staining for DP. (A)** Schematic depicting the location of cells for which nuclear DP was assessed. The gray rectangular area (with dashed lines) shows area adjacent to migration front edge. The black rectangular area (with dashed lines) shows area at migration front edge. **(B–E)** DP accumulates in nucleus with the loss of K6a/K6b both in areas adjacent to the migration front edge and in areas at the migration front edge. DP, red; DAPI, blue. Arrows point to the direction of migration. Arrowheads point to examples of nuclear-localized DP. Bars, 100 µm.

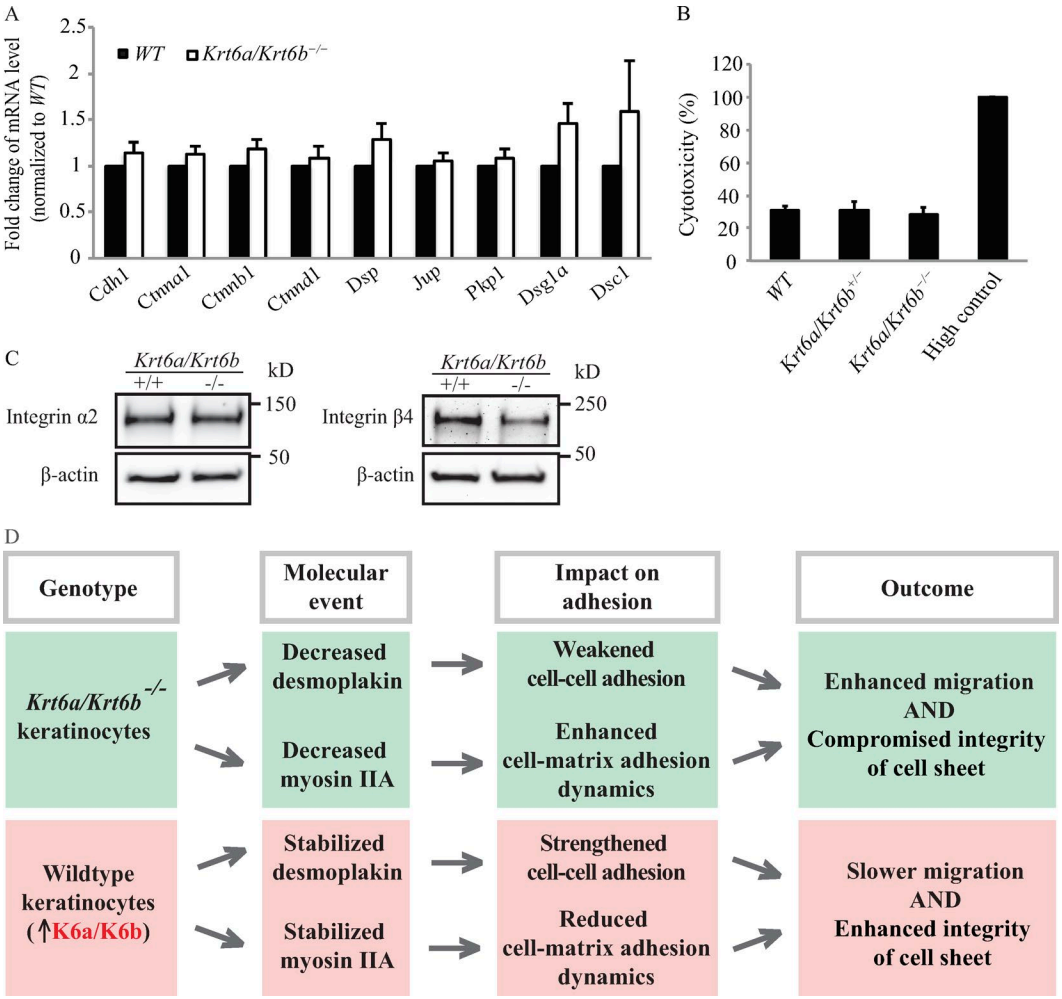

Figure S5. **Loss of K6a/K6b did not affect either the mRNA levels of genes that encode proteins at cell–cell adhesions or cell fragility, but it led to down-regulation of integrin β4 protein level. (A)** By qRT-PCR, WT and *Krt6a/Krt6b*-null keratinocytes from 6-d skin explant culture were similar with respect to the mRNA levels of genes that encode certain proteins at adherens junctions and desmosomes. *Gapdh* and *Rn18s* were used as loading controls. Data represent the mean + SEM of three biological replicates. **(B)** WT and *Krt6a/Krt6b*-null keratinocytes exhibited a similar degree of cytolysis in the dispase-based assay. Cytotoxicity was assessed via the LDH release assay. The data shown represent the mean + SEM of three biological replicates. **(C)** Western blot analysis of whole-cell lysates harvested from 6-d skin explant culture showed that *Krt6a/Krt6b*-null keratinocytes had a reduced level of integrin β4. β-Actin was used as a loading control. *n* = 4 biological repeats. **(D)** Schematic depicting possible mechanism through which K6a/K6b impacts keratinocyte collective migration. After injury, K6a/K6 proteins are rapidly induced in surviving keratinocytes proximal to the wound to optimize cell–cell and cell–matrix adhesion toward efficient wound reepithelialization. Although the absence of K6 leads to increased migration by destabilizing cell–cell and cell–matrix adhesion, the resulting loss in the integrity of the keratinocyte sheet may delay or impair wound healing.

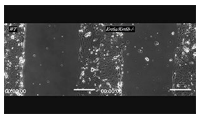

Video 1. **Loss of K6a/K6b leads to accelerated keratinocyte collective migration.** Representative phase-contrast time-lapse videos of WT (left) and *Krt6a/Krt6b*-null (right) keratinocytes migrating on type I collagen (corresponds with Fig. 1 D). Compared with WT keratinocytes, *Krt6a/Krt6b*-null keratinocytes migrate over a larger surface area. Cells were imaged every 10 min for 16 h using an AxioObserver Z1 microscope equipped with an EC Plan Neofluar 10×/0.3 Ph1 objective. Timestamp is displayed in the hh:mm:ss format. Bar, 200 µm.

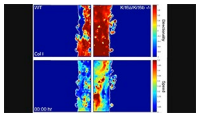

Video 2. **Spatial mapping of directionality and speed of WT and *Krt6a/Krt6b*-null keratinocytes migrating on type I collagen by PIV analysis.** The motion directionality is shown by cos(θ) of the velocity vectors, and speed is the absolute value of velocities. As indicated by color, directionality (top) was largely similar across either WT (left) or *Krt6a/Krt6b*-null (right) cell sheets, indicating that the motion was mostly collective and that keratinocytes migrated as a sheet instead of groups of cells. Compared with *Krt6a/Krt6b*-null cells, WT cells were less coordinated in the first half time (before 8 h), but their coordination improved in the later times. *Krt6a/Krt6b*-null cells migrated faster (Fig. 1 F) than WT cells, resulting in increased migration area as illustrated in Fig. 1 E.

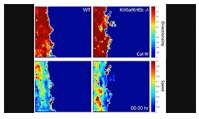

Video 3. **Spatial mapping of directionality and speed of WT and *Krt6a/Krt6b*-null keratinocytes migrating on type IV collagen by PIV analysis.** The motion directionality is shown by cos(θ) of the velocity vectors, and speed is the absolute value of velocities. WT (left) and *Krt6a/Krt6b*-null (right) keratinocytes exhibited similar directionality (top) on type IV collagen, which validates the quantification result shown in Fig. 1 G. Although cell directionality between two genotypes was similar, *Krt6a/Krt6b*-null cells showed modestly enhanced migration speed (see Fig. 1 F) compared with WT cells, especially for the cells inside the cell sheet.

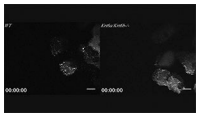

Video 4. **Loss of K6a/K6b enhances focal adhesion turnover in keratinocytes migrating on type I collagen.** Representative time-lapse videos of mCherry–paxillin dynamics in WT (left) and *Krt6a/Krt6b*-null (right) cells migrating on type I collagen (corresponds with Fig. 2, F–H). In both WT and *Krt6a/Krt6b*-null keratinocytes, focal adhesion first appeared at the extending leading edge and then matured and slid toward the center of actively migrating cells. The maturation stage seemed to be much shorter with the loss of K6a/K6b. Cells were imaged every 3 min for ∼3 h using an AxioObserver Z1 microscope equipped with an EC Plan Neofluar 40×/1.30 oil DIC M27 objective. Timestamp is displayed in the hh:mm:ss format. Bar, 20 µm.

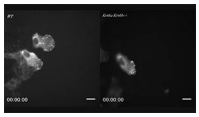

Video 5. **The rate of focal adhesion turnover is similar between WT and *Krt6a/Krt6b*-null keratinocytes on type IV collagen.** Representative time-lapse videos of mCherry–paxillin dynamics in WT (left) and *Krt6a/Krt6b*-null (right) cells migrating on type IV collagen (corresponds with Fig. 2 I). Cells were imaged every 3 min for ∼3 h using an AxioObserver Z1 microscope equipped with an Plan Apochromat 63×/1.40 oil DIC M27 objective. Timestamp is displayed in the hh:mm:ss format. Bar, 20 µm.

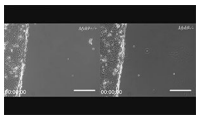

Video 6. **Myh9 deletion results in altered cell–cell adhesion at the migration front of keratinocyte sheets.** Representative phase-contrast time-lapse videos of $Myh9^{+/+}$ (left) and $Myh9^{-/-}$ (right) keratinocytes migrating on type I collagen (corresponds with Fig. 3, H–J). After removal of the culture insert, $Myh9^{+/+}$ cells (left) at the edge of the insert become the leader cells and were always migrating at the very front of the collective migrating cells. Cell–cell adhesions were dynamically changing within the $Myh9^{-/-}$ keratinocyte sheet (right). As such, some follower cells that were initially behind the migration leading edge were sometimes able to squeeze past the leader cells to arrive at the very front, thus becoming the new leader cells. Cells were imaged every 10 min for 16 h using an AxioObserver Z1 microscope equipped with an EC Plan Neofluar 10×/0.3 Ph1 objective. Timestamp is displayed in the hh:mm:ss format. Bar, 200 µm.

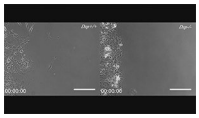

Video 7. ***Dsp* deletion results in enhanced keratinocyte collective migration.** Representative phase-contrast time-lapse videos of $Dsp^{+/+}$ (left) and $Dsp^{-/-}$ (right) keratinocytes migrating on type I collagen (corresponds with Fig. 4 H). $Dsp^{-/-}$ cells (right) migrated at an enhanced rate compared with $Dsp^{+/+}$ cells (left). Cells were imaged every 10 min for 16 h using an AxioObserver Z1 microscope equipped with an EC Plan Neofluar 10×/0.3 Ph1 objective. Timestamp is displayed in the hh:mm:ss format. Bar, 200 µm.